JOURNAL OF SPACECRAFT AND ROCKETS
Vol. 47, No. 5, September–October 2010

Loosely Coupled Simulation for Two-Dimensional Ablation and Shape Change

Yih-Kanq Chen* and Frank S. Milos†
NASA Ames Research Center, Moffett Field, California 94035-1000
and
Tahir Gökçen‡
ELORET Corporation, Sunnyvale, California 94086

DOI: 10.2514/1.39667

The central focus of this study is to demonstrate that time-accurate solutions for multidimensional ablation and shape change of thermal protection system materials may be obtained by loose coupling of a high-fidelity flow solver with a material thermal response code. In this study, the flow code solves the nonequilibrium Navier–Stokes equations using the data-parallel line-relaxation (DPLR) method. The material response code is the latest version of the Two-dimensional Implicit Thermal Response and Ablation Program (TITAN). In TITAN, the governing equations, which include a three-component decomposition model and a surface energy balance with thermochemical ablation, are solved with a robust moving-grid scheme to predict the shape change caused by surface recession. Coupling between the material response and flow codes is required for many multidimensional ablation simulations, because the magnitude and distribution of the surface heat flux are very sensitive to shape change. This paper demonstrates the application of the TITAN-DPLR system to problems with large-scale recession and shape change. Ablation and thermal response simulations are presented for iso-*q* and flat-faced arc-jet test models and also for a wedge with a cylindrical leading edge exposed to hypersonic flow at various angles of attack.

Nomenclature

A	=	area, m^2
B	=	reaction preexponential constant in Eq. (3), s^{-1}
B'	=	nondimensional mass blowing rate
C_H	=	Stanton number for heat transfer
C_M	=	Stanton number for mass transfer
c_p	=	specific heat, J/kg-K
D	=	species diffusion velocity, m/s
E	=	total energy per unit volume, J/m^3
E/R	=	reaction activation temperature, K
H_r	=	recovery enthalpy, J/kg
h	=	enthalpy, J/kg
$\bar{h}$	=	$(\rho_v h_v - \rho_c h_c)/(\rho_v - \rho_c)$, J/kg
k	=	thermal conductivity, W/m-K
$\dot{m}$	=	mass flux, kg/m^2-s
n	=	number of gaseous species
Q_{T-v}	=	translation-vibration energy exchange rate, W/m^3
q	=	heat flux, W/m^2
q_{cond}	=	conduction heat flux, W/m^2
q_r	=	radiative heat flux, W/m^2
T	=	temperature, K
T_∞	=	environment temperature for radiation, K
t	=	time, s
u	=	gas velocity, m/s
v	=	local grid velocity, m/s
w	=	source term in Eq. (8), kg/m^3-s
x, y	=	Cartesian coordinate system, m
z	=	mass fraction of virgin material
α	=	absorptivity
Γ	=	volume fraction of resin
ε	=	surface emissivity
λ	=	blowing reduction parameter
ξ, η	=	general body-fitted coordinates, m
ρ	=	total density, kg/m^3
σ	=	Stefan–Boltzmann constant, W/m^2-K^4
τ	=	shear stress, N/m^2
Φ	=	porosity
ψ	=	reaction order

Subscripts

c	=	char
e	=	edge
g	=	pyrolysis gas
i, j	=	direction components
k	=	density component (A, B, and C)
s	=	gas species
v	=	virgin or vibrational energy
w	=	wall
1	=	unblown (C_{H1})

Presented as Paper 2008-3802 at the 41st Thermophysics Conference, Seattle, WA, 21–24 June 2008; received 9 July 2008; revision received 1 July 2010; accepted for publication 1 July 2010.

*Aerospace Engineer, Aerothermodynamics Branch, Mail Stop 230-2. Member AIAA.
†Aerospace Engineer, Thermal Protection Materials Branch, Mail Stop 234-1. Senior Member AIAA.
‡Senior Research Scientist. Senior Member AIAA.

I. Introduction

VEHICLES designed for Earth entry at superorbital velocities, as well as those designed for ballistic entry at orbital velocities, typically use thermal protection system (TPS) materials that pyrolyze and ablate at high temperature for mass-efficient rejection of the aerothermal heat load. phenolic impregnated carbon ablator (PICA) [1] is one of the light-weight ceramic charring ablators developed at the NASA Ames Research Center in the early 1990s. PICA was the heat-shield material on the Stardust probe [2], which is, to date, the fastest man-made Earth-entry space vehicle. PICA was also a candidate TPS material for the Orion Crew Module [3].

The effects of multidimensional heat conduction in PICA were studied in previous papers [4,5]. These effects are important in stagnation arc-jet models and in the shoulder region of the Orion heat shield. For these geometries, simple one-dimensional analyses using tools such as the Fully Implicit Ablation and Thermal Response

(FIAT) code [6] or Charring Material Ablation (CMA) code [7] may not be adequate. The two-dimensional TITAN code [8] was upgraded [5] to provide a capability for improved fidelity and TPS sizing, including nonisotropic thermal conductivity, a common feature of TPS materials.

The previous work considered only uncoupled analysis, where the effect of shape change is not taken into account in the computational fluid dynamics (CFD) analysis of the external flowfield. This approach is reasonable for a large blunt vehicle such as the Orion Crew Module, and it may be adequate for some arc-jet cases in which relative shape change is small. However, in general, the magnitude and distribution of heat flux are very sensitive to the shape of the TPS surface geometry, and a coupled fluid-solid analysis should be performed if the shape change is significant. That is, the changes in aeroheating distributions that result from shape change should be determined as part of the calculation.

Aerotherm Corporation developed ABRES Shape Change Code (ASCC), which is an engineering code for coupled solid–fluid simulation of axisymmetric or planar two-dimensional geometries [9]. In ASCC, internal decomposition is not implemented, and the thermal diffusion equation is solved using a finite difference scheme with overlaid grids that is not always accurate. To address these deficiencies, the authors developed the TITAN program to perform high-fidelity thermal response and shape-change simulations for charring materials [8]. Its governing equations, which include a three-component decomposition model with a moving grid, are discretized using a finite volume approximation with general body-fitted coordinates. A time-accurate solution is achieved by an implicit time-marching technique using Gauss–Seidel line relaxation with alternating sweeps.

In many applications, a coupled fluid-solid simulation is required for accurate prediction of ablative shape change. In previous work, the Gauss–Seidel Implicit Aerothermodynamic Navier–Stokes Code (GIANTS) [10] and the momentum energy integral technique (MEIT) [11] were integrated with TITAN using a loosely coupled method for simulation of solid–fluid interaction. MEIT provides surface heat flux predictions for slender sphere-cone geometries; however, the accuracy is poor for blunt geometries. Thus, the TITAN-MEIT system can only be used to solve a small number of problems. The GIANTS code can generate accurate solutions by solving the full Navier–Stokes equations, but its line-relaxation iteration scheme is relatively inefficient. In principle, the TITAN-GIANTS code can be used for general two-dimensional ablation simulations, but excessive computational time makes it impractical to use TITAN-GIANTS to perform parametric studies in support of TPS testing and design.

The Navier–Stokes CFD code, developed at NASA Ames Research Center, uses the state-of-the-art DPLR method [12]. DPLR is a message-passing-interface-based full three-dimensional Navier–Stokes solver. DPLR was developed specifically for fast, robust, and accurate solutions to hypersonic entry problems of interest to NASA. The code includes a large selection of generalized surface boundary conditions and hooks to enable efficient loose coupling with a TPS material response code. The solution accuracy may also be improved, because the discretization scheme of DPLR is less dissipative than that of GIANTS.

The purpose of this paper is to present the new TITAN-DPLR simulation system and its applications to ablative shape-change simulations. The coupling technique between TITAN and DPLR is similar to that used previously for TITAN and GIANTS. On computer systems with multiple processors to enable parallel processing, TITAN-DPLR solves ablation problems with just a small fraction of the time required by TITAN-GIANTS. Since DPLR is a general three-dimensional flow solver, a three-dimensional coupled simulation may also be feasible if TITAN is replaced with 3dFIAT [13].

Four test cases are investigated in this paper to explore the capabilities of the TITAN-DPLR integrated system. The test cases are 1) an axisymmetric sphere cone with 10° half-angle, 2) a two-dimensional cylinder wedge at various angles of attack, 3) an axisymmetric flat-faced arc-jet model, and 4) an axisymmetric iso-q-shaped arc-jet model, which is made up of a spherical segment nosecap, with nose radius equal to the model diameter, and a cylindrical body aligned with the flow. In cases 3 and 4, the predictions using the loosely coupled technique are compared with those obtained without such coupling. The comparisons include shape change, surface heating, and in-depth thermocouple temperature history. Comparisons with experimental data for arc-jet stagnation models are presented in the papers by Milos and Chen [5] and by Gökcen et al. [14].

II. Computational Methods

In this section we describe the relevant equations of the TITAN and DPLR codes and the loose-coupling procedure employed to obtain the solutions presented in this work.

A. Material Ablation and Thermal Response

The governing equations in TITAN, which include energy conservation, a three-component decomposition model, and the surface energy balance, are solved with a moving-grid system to simulate the shape change due to surface recession. The equations are converted from a Cartesian coordinate system (x, y) into a general body-fitted coordinate system (ξ, η) and then discretized using a finite volume method. An improved moving-grid technique was implemented to better solve simulations with large recession.

The internal energy balance is a transient thermal conduction equation with additional pyrolysis terms:

$$\rho c_p \frac{\partial T}{\partial t} = \nabla \cdot (k \nabla T) - (h_g - \bar{h}) \nabla \cdot \dot{m}_g - \dot{m}_g \cdot \nabla h_g + \rho c_p v \cdot \nabla T \quad (1)$$

The individual terms in Eq. (1) may be interpreted as follows: the rate of storage of sensible energy, the net rate of thermal conductive heat flux, the pyrolysis energy-consumption rate, the net rate of energy convected by pyrolysis gas, and the convection rate of sensible energy due to coordinate system movement.

Most ablative TPS materials are organic resin composites. The composite solid is modeled as a general mixture of a two-component resin and a reinforcing material. The local density of the solid is given by the equation:

$$\rho = (1 - \Phi)(\Gamma(\rho_A + \rho_B) + (1 - \Gamma)\rho_C) \quad (2)$$

where A and B represent components of the organic resin, and C represents the reinforcing material. The porosity Φ and resin volume fraction Γ are input quantities. Each of the three components may decompose independently by an Arrhenius-type reaction rate:

$$\frac{\partial}{\partial t}\left(\frac{\rho_k - \rho_{ck}}{\rho_{vk}}\right) = -B_k \left(\frac{\rho_k - \rho_{ck}}{\rho_{vk}}\right)^{\psi_k} e^{(-E_k/RT)} + \frac{v \cdot \nabla \rho_k}{\rho_{vk}} \qquad k = A, B, C \quad (3)$$

where ρ_{vk} and ρ_{ck} are the original (virgin) and the residual (char) density, respectively, of component k. The assumption of independent reactions is consistent with results from thermogravimetric analysis.

Virgin and char density and thermal properties $(c_p, k, \alpha, \varepsilon)$ are specified as functions of temperature and, if necessary, pressure and orientation. The virgin and char states are well defined, and most properties may be measured over some range of conditions. The char thermal conductivity is an exception, because samples from relevant environments (arc jet or flight) tend to be too small or inhomogeneous. Therefore, this property typically is estimated by tuning the predicted thermal response to match temperature histories measured in arc-jet tests. The pyrolysis-gas enthalpy h_g is input as a function of temperature and pressure. The thermal and mechanical properties of some heat-shield materials are available in the TPS*X* Material Properties Database [15].

The thermal properties of partially charred states are not uniquely defined, because any intermediate density may be reached by different time–temperature histories. The properties of such states are

also impractical to measure, because of chemical instability of the material in the temperature range of interest. The properties of partially charred material are obtained by interpolation of the specified virgin and char properties using density as an independent variable to circumvent these difficulties. For example, in the partially pyrolyzed zone ($\rho_c < \rho < \rho_v$), the specific heat is obtained from the mixing rule:

$$c_p = zc_{pv} + (1 - z)c_{pc} \tag{4}$$

where

$$z = \frac{(1 - \rho_c/\rho)}{(1 - \rho_c/\rho_v)}$$

In the above equation, the subscripts v and c denote the virgin and char properties, respectively, and z is the mass fraction of virgin material (in a theoretical mixture of virgin and char) that yields the correct local density ρ. This model enables the material properties to transition smoothly from the virgin state ($z = 1$) to the char state ($z = 0$) using uniquely defined properties that are bounded by the two specified states. The thermal conductivity is weighted in the same manner.

Pyrolysis-gas flow is assumed to be quasi-steady and one-dimensional in the η direction. The pyrolysis gas is assumed to be in thermal equilibrium with the porous solid (partially or fully charred) through which it is flowing. If the inner boundary is impermeable, then outward pyrolysis-gas mass flux may be calculated as

$$\dot{m}_g = -\frac{1}{A}\int_{\eta_0}^{\eta} \frac{\partial \rho_s}{\partial t} A \, \mathrm{d}\eta \tag{5}$$

where η_0 is located at the inner boundary, and $A(\eta)$ is the cross-sectional area.

Conditions at the ablating surface are determined by the aerothermal environment and by chemical interactions between the boundary-layer gas, the pyrolysis gas, the ablation products, and the chemical constituents of the surface material. TITAN employs a convective-transfer-coefficient form of the surface energy balance:

$$\rho_e u_e C_H (H_r - h_w) + \dot{m}_c h_c + \dot{m}_g h_g - (\dot{m}_c + \dot{m}_g) h_w + \alpha_w q_{rw} - \sigma \varepsilon_w (T_w^4 - T_\infty^4) - q_{\text{cond}} = 0 \tag{6}$$

Here, $\rho_e u_e C_H$ is the convective heat transfer coefficient, H_r is the recovery enthalpy, and all other quantities are defined at the ablating surface. The first term in Eq. (6) is the convective heat flux, the second through fourth terms represent the chemical energy released (or absorbed) by ablation, the fifth and sixth terms are radiation absorption and emission, respectively, and the final term is the rate of heat conduction into the TPS. This equation has been simplified from the general form [6] by assuming equal diffusion coefficients within the boundary layer and equal Stanton numbers for heat and mass transfer. These are standard assumptions for most entry environments and TPS materials. If these assumptions are not applicable, a more general form of the surface energy balance may be used. Flowfield radiation is reflected or absorbed at the surface, but not transmitted.

A blowing correction accounts for the reduction in heat transfer coefficient due to the injection of gases from pyrolysis and surface ablation into the boundary layer. The blowing correction equation used by TITAN is

$$\frac{C_H}{C_{H1}} = \frac{\ell_n (1 + 2\lambda B')}{2\lambda B'} \tag{7}$$

where

$$B' = \frac{(\dot{m}_c + \dot{m}_g)}{\rho_e u_e C_M}$$

λ is the blowing reduction parameter, and C_H/C_{H1} is the ratio of the blown (ablating) to the unblown (nonablating) heat transfer coefficients. For laminar flow, λ is 0.5 or higher, depending on the geometry and the ratio of molecular weights of the injected and boundary-layer-edge gas. For transitional or turbulent flow, smaller values of λ are used. B' is the nondimensional mass blowing rate at the surface. Unless noted otherwise, a blowing reduction parameter of 0.5 is used for the calculations presented herein.

In the preceding equations, the input quantities are H_r, $\rho_e u_e C_{H1}$, α_w, ε_w, λ, and q_r. The solution variables are $\dot{m}_g$, q_{cond}, and T_w. Therefore, $\dot{m}_c$ and h_w are the only additional unknowns. Tables of B'_c and h_w for ablative materials may be generated using the Aerotherm Chemical Equilibrium (ACE) or Multicomponent Ablation Thermochemistry (MAT) codes [16,17]. Mechanical erosion is ignored. In general, for pyrolyzing ablators B'_c is a complex function of temperature, pressure, and B'_g.

A one-block grid system is not adequate to simulate the conditions studied in this work because of the near-surface pyrolysis-gas flow and the moving grid. Thus, a two-block grid system is adopted. A typical two-block computational domain for TITAN is shown in Fig. 1. The computational grid system is initially generated based on the unablated shape of TPS material. then as ablation occurs, the surface grid points move with the receding surface, and the interior points are reconstructed accordingly. The computational domain is divided into three regions, labeled a, b, and c in Fig. 1. For a given time step, the new surface grid points are determined based on the local surface recession rate then new locations for internal grid points are calculated using two different approaches. In the first approach, the new grid system is rebuilt by compressing regions a and b in user specified direction; however, the grid points in region c remain unchanged. In the second approach, the moving speeds of the interfaces between regions a and c and between regions b and c are specified (usually less than or equal to the stagnation-point recession rate), and the internal grid points are moved accordingly. The second approach is more robust for simulations with large-scale recession, but requires more computational time. Once the new location of a grid point is determined, the local grid velocity, v, is defined as the ratio of moving distance of this point and the time step. then the moving-grid terms (the last term on the right hand side) in Eqs. (1) and (3) can be determined. Details of the moving-grid scheme can be found in [8].

B. Fluid Dynamics

The Navier–Stokes solver, DPLR, is used to estimate the hypersonic aeroheating distribution over a blunt body [12]. The governing equations may be characterized as representing a flowfield in thermal and chemical nonequilibrium. The DPLR code solves the time-dependent conservation equations of mass, momentum, and energy within the flowfield. The species mass conservation equation is given by

$$\frac{\partial \rho_s}{\partial t} + \frac{\partial}{\partial x_j}(\rho_s u_j) = -\frac{\partial}{\partial x_j}(\rho_s D_{sj}) + w_s \tag{8}$$

The total momentum conservation is written as

$$\frac{\partial}{\partial t}(\rho u_i) + \frac{\partial}{\partial x_j}(\rho u_i u_j) = -\frac{\partial \tau_{ij}}{\partial x_j} \tag{9}$$

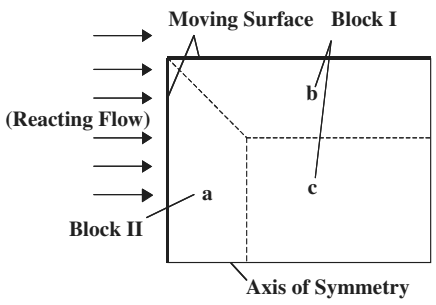

Fig. 1 TITAN computational domain with two blocks and three regions.

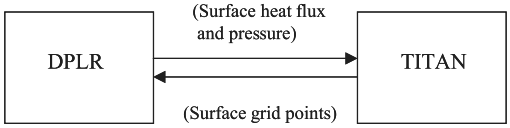

Fig. 2 Flowchart for a loosely coupled computation.

and the vibrational and total energy equations are written as

$$\frac{\partial E_v}{\partial t} + \frac{\partial}{\partial x_j}(E_v u_j) = -\frac{\partial}{\partial x_j}(q_{vj}) + Q_{T-v} \frac{\partial E}{\partial t} + \frac{\partial}{\partial x_j}((E+p)u_j)$$
$$= -\frac{\partial}{\partial x_j}(q_j + q_{vj}) - \frac{\partial}{\partial x_j}(u_i \tau_{ij}) - \sum_{s=1}^{n} \frac{\partial}{\partial x_j} D_{sj} h_s \qquad (10)$$

In DPLR, the Gauss–Seidel line relaxation method is modified to enable fast convergence for viscous flow with high parallel efficiency on massively parallel computers.

C. Loose Coupling

The integration between TITAN and DPLR is based on a loosely coupled approach following the flowchart presented in Fig. 2. In this approach, all CFD solutions are computed for an unblown surface but use the ablated shape. Surface thermochemical interactions and blowing effects are incorporated in the material response code by use of ablation tables, the surface energy balance with heat transfer coefficient, and the blowing reduction parameter, as described by Eqs. (6) and (7).

All calculations presented in this work are with constant flow condition representing arc-jet test conditions. The initial flow field and its associated surface heat flux and pressure are first computed by DPLR. For each surface point, heat transfer coefficient C_{H1} is calculated. Then pressure and heat transfer coefficient are passed as boundary conditions to TITAN. A time-accurate ablation and thermal response computation is performed by TITAN. When the maximum surface recession meets a prespecified limit, TITAN stops its computation and outputs the location of the ablated surface. A new CFD grid is then generated based on this ablated surface and estimated shock location, and a new steady-state flow solution is then calculated by DPLR. The pressure and heat transfer coefficients are calculated for this new solution. The updated values for pressure and heat transfer coefficients are input to TITAN for another run of time-accurate ablation and in-depth thermal response. This procedure is repeated until TITAN reaches the specified final time. In each CFD run, the outer boundary of grid is aligned with the shock using an internal subroutine in DPLR, and the cell Reynolds number equal to 1 is enforced.

The TITAN-DPLR loose-coupling procedure is written in a UNIX/Linux script file. The test cases presented in this paper are computed on a UNIX cluster system containing 124 nodes.

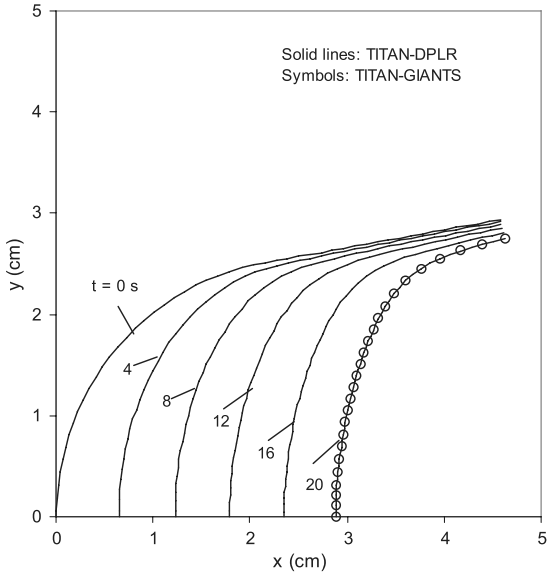

Fig. 3 Surface contours at various times for case I.

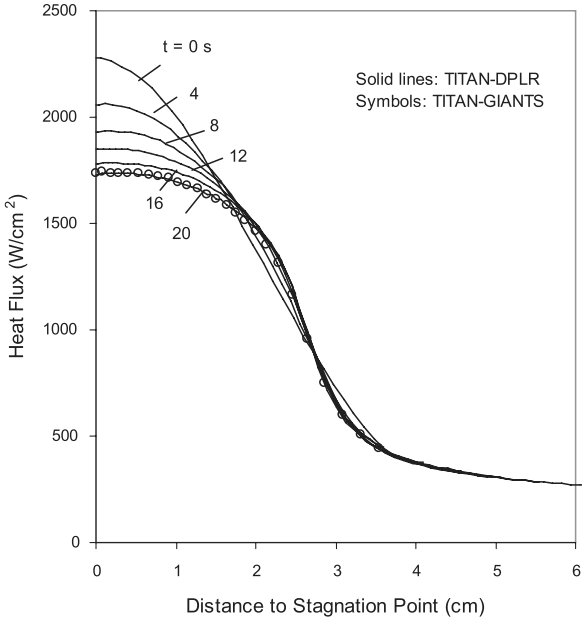

Fig. 4 Surface heat flux distributions at various times for case I.

III. Results

Four test cases are presented in this section to demonstrate the capabilities of the TITAN-DPLR system. The first case considers the surface recession of a 10° half-angle sphere cone, and the TITAN-DPLR solution is compared with an existing TITAN-GIANTS solution. The second case is flow at angle of attack over a two-dimensional cylinder wedge. The purpose of this case is to study the effect of angle of attack on the ablated shape. The third and fourth cases consider the ablation of axisymmetric flat-faced and iso-q-shaped arc-jet models, respectively, under typical NASA Ames arc-jet stream conditions. For all four cases, we discuss details of the computational procedures and the predicted time-accurate solutions.

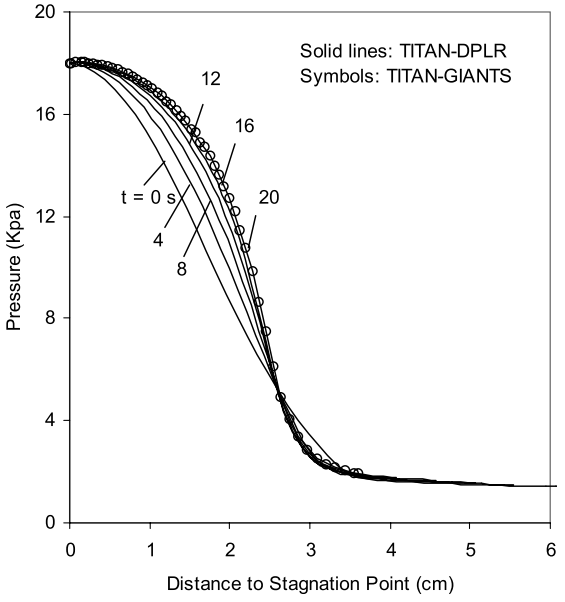

Fig. 5 Surface pressure distribution at various times for case I.

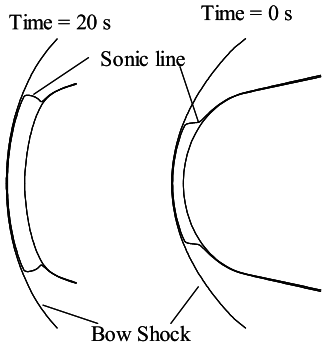

Fig. 6 Bow shock and sonic line for case I.

PICA material properties are used for all cases, but the methodology applies to other ablative materials as well.

A. Case I

An axisymmetric 10° half-angle sphere cone with nose radius of 2.54 cm is studied. The purpose of this exercise is to check code consistency and to compare predictions with a TITAN-GIANTS solution. The initial stagnation-point heat flux is 2.28 kW/cm^2, and the stagnation-point pressure is 18 kPa. The DPLR simulation has a grid size of 50×149, and the TITAN computation has a grid size of 52×160. Loose coupling is performed to achieve a time-accurate shape-change prediction. Aerothermal environments, including heat flux and pressure, are updated when the maximum surface recession at any point exceeds 0.005 cm. Based on previous experience, this criterion is believed to be adequate for obtaining a time-accurate prediction.

The predicted surface contours at $t = 0$, 4, 8, 12, 16, and 20 s are shown in Fig. 3. The corresponding surface heating and pressure

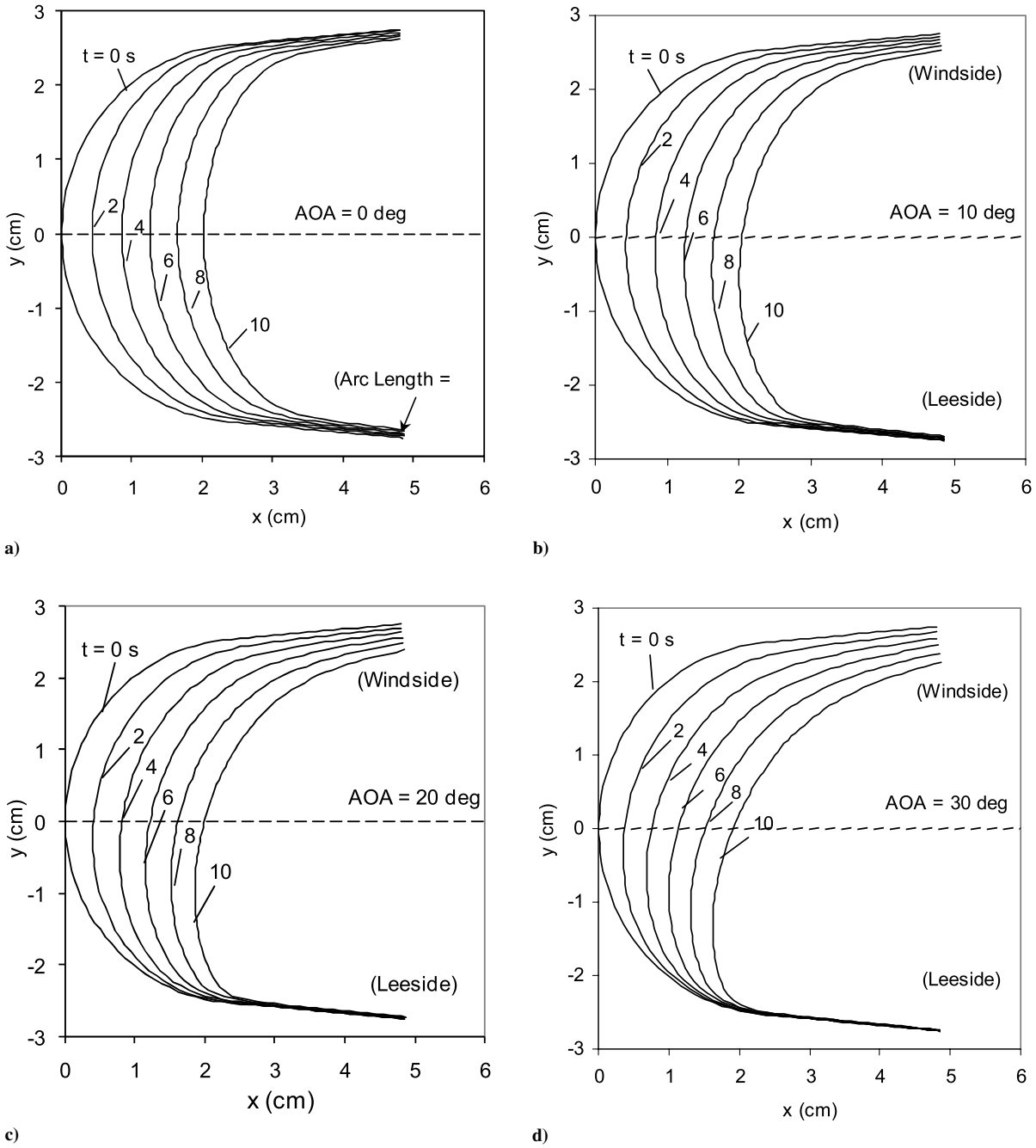

Fig. 7 Surface contours at various times for case II with a) AOA = 0°, b) AOA = 10°, c) AOA = 20°, and d) AOA = 30°.

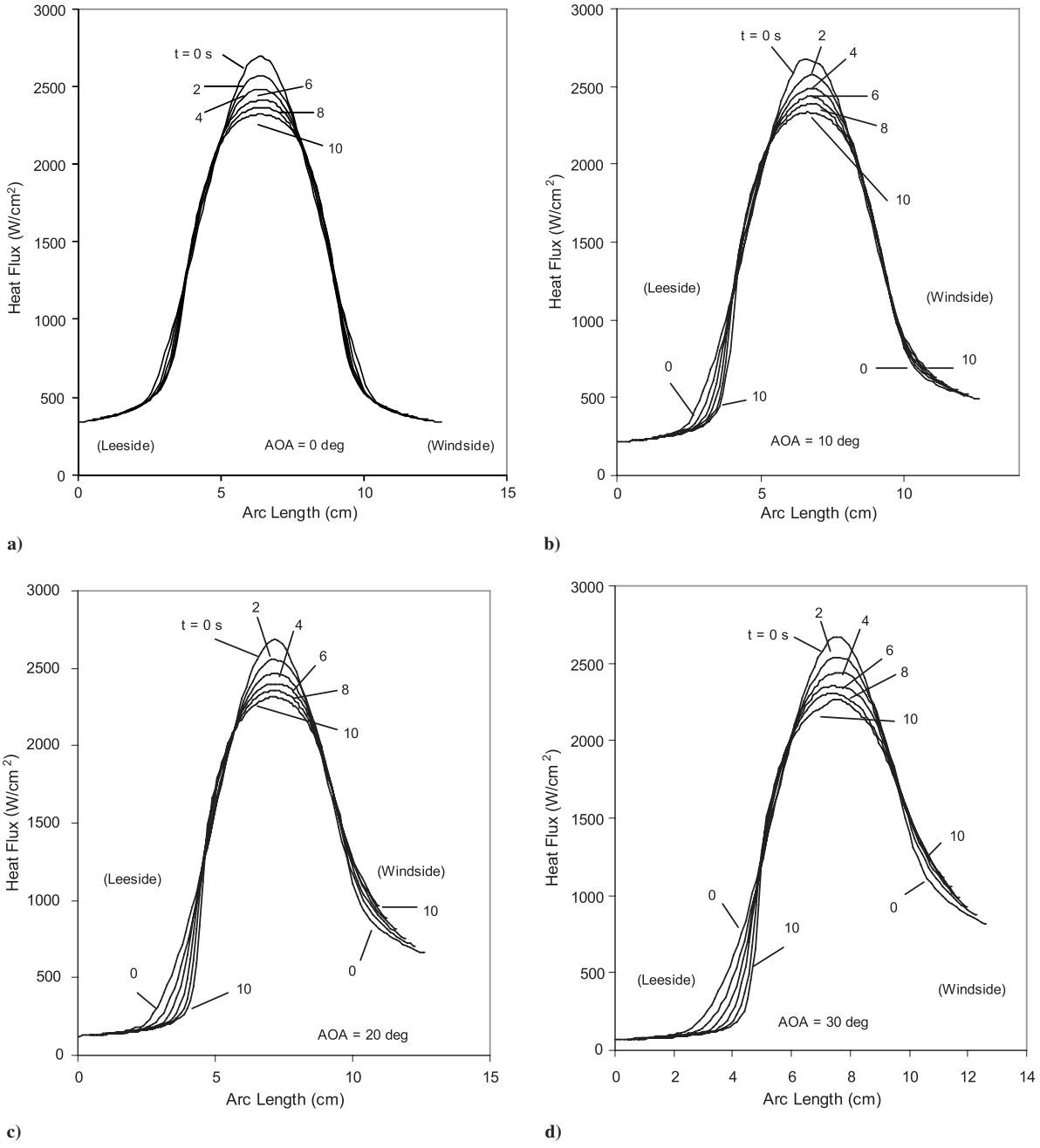

Fig. 8 Surface heat flux at various times for case II with a) AOA = 0°, b) AOA = 10°, c) AOA = 20°, and d) AOA = 30°.

distributions are presented in Figs. 4 and 5, respectively. At the end of simulation ($t = 20$ s), the stagnation-point recession is 2.9 cm, and the heat flux decreased to 1.73 kW/cm^2. The stagnation pressure does not change, because the freestream conditions are constant. As expected, the spherical nose becomes blunter and the stagnation heat flux decreases as a function of time. Consequently, the stagnation-point recession rate declines as a function of time.

A comparison between TITAN-DPLR and TITAN-GIANTS at the final time is included in Figs. 3 and 4. The predicted shape change and heat flux distribution from TITAN-DPLR are in excellent agreement with those from TITAN-GIANTS (symbols). For this test case, the computation time for the TITAN-DPLR system is about 5% of that for the TITAN-GIANTS system. The difference in CPU time will, of course, vary with the number of processors used in the DPLR computation.

Figure 6 shows Mach and shock contours at $t = 0$ and 20 s. The subsonic zone at $t = 20$ s is much greater than that at $t = 0$. This is because the sonic point moves farther downstream as the spherical nose becomes blunter, and at the same time, the bow shock moves further away from the surface.

B. Case II

This simulation is performed to predict the interaction between a hypersonic airstream and a two-dimensional 5° half-angle cylinder wedge at various angles of attack (AOA). The radius of the cylinder is 2.54 cm. The initial stagnation-point heat flux is 2.67 kW/cm^2, and the stagnation-point pressure is 60 kPa. The DPLR simulation has a grid size of 100 × 149, and the TITAN calculation has a grid size of 102 × 160.

The surface contours at various times (0, 2, 4, 6, 8, and 10 s) for four different fixed AOA (0, 10, 20, and 30°) are presented in Figs. 7a–7d, respectively. The corresponding surface heating distributions are shown in Figs. 8a–8d. Ablation removes solid material and reshapes the surface geometry. This process leads to highly asymmetric geometry at large angle of attack. As the surface recedes,

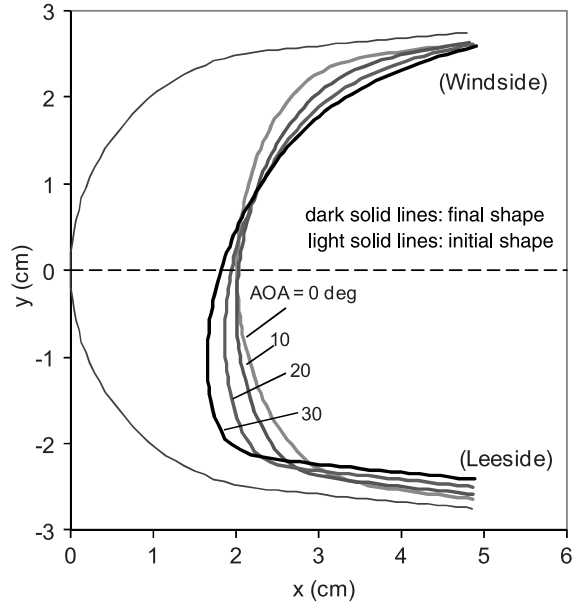

a)

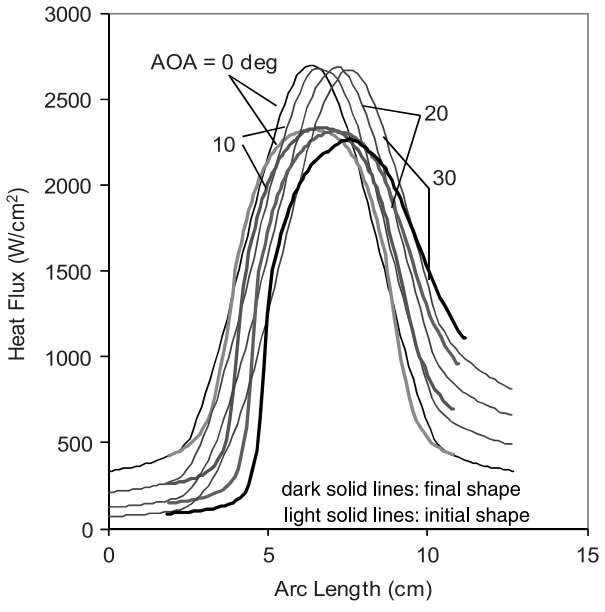

b)

Fig. 9 Plots of a) surface contours at 10 s for case II with various AOA and b) surface heat flux at 10 s for case II with various AOA.

the heat flux around the stagnation region gradually decreases. The heat flux on the windward-side wedge surface increases as a function of time, whereas on the leeward-side wedge surface the heat flux decreases.

To better present the comparison of shape change and heating distribution among these four AOA, the initial ($t = 0$) and final ($t = 10$ s) surface contours for these four AOA are plotted in Fig. 9a. The corresponding surface heating distributions are plotted in Fig. 9b. The final surface shape, as expected, strongly depends on angle of attack. The shape becomes more asymmetric as the AOA is increased. For all AOA studied here, the total stagnation-point recession is about the same at 2.0 cm. Additionally, the final stagnation heat flux for all cases is at around 2.35 kW/cm^2, which is equivalent to a 13% reduction relative to the initial value.

Figure 10 shows the shock shape and sonic line for AOA $= 20°$ at $t = 0$ and 10 s. Material ablation significantly alters the surface shape and increases the area of the subsonic zone. These changes lead to a reduction of the velocity gradient and heat flux at the stagnation

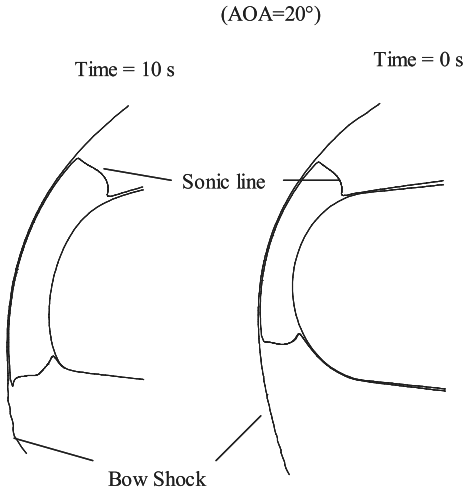

Fig. 10 Bow shock and sonic line for case II.

point. Flowfield predictions for other AOA have the same trend and are not presented due to space limitations.

C. Case III

Flat-faced models are frequently used in arc-jet tests. For this case, a TITAN-DPLR analysis is performed for an arc-jet model with a cylindrical radius of 5.08 cm and a shoulder radius of 0.635 cm. The initial stagnation-point heat flux is 810 W/cm^2, and the stagnation-point pressure is 20 kPa. The DPLR computation has a grid size of 221×149, and the TITAN simulation has a grid size of 223×160.

The predicted surface contours at various times are shown in Fig. 11a, and the relative shape change after 20 s of exposure to the arc stream is illustrated in Fig. 11b. A comparison of surface heating distributions between $t = 0$ and $t = 20$ s is presented in Fig. 12. The peak heat flux on the shoulder at $t = 0$ is 1.35 kW/cm^2, which is approximately 67% higher than the stagnation heat flux. The surface recession in the stagnation region is thus lower than the recession in the shoulder region. The shoulder recession increases the local radius of curvature and consequently reduces the local heat flux. At the end of the 20 s exposure, the heat flux in the shoulder region decreases about 20% compared with the initial value. On the other hand, the stagnation-point heat flux increases by about 22% relative to its initial value.

For the ablated shape, the DPLR heat flux distribution has a spatial oscillation in the shoulder region. This oscillation was not seen in the first two cases or in similar TITAN-GIANTS solutions. The source of oscillation is DPLR. Further study is required to resolve this issue. These minor perturbations in surface heat flux should not have a significant impact on the accuracy of in-depth material simulation for this case. Even though DPLR is much faster than GIANTS, the computation time for this case is still enormous (around 90 h), primarily because of a fairly large subsonic area in the front of the model. Figure 13 shows the sonic line and shock contours at $t = 0$ and 20 s. The shock standoff distance decreases as the model ablates, the effective radius decreases and consequently the stagnation-point heat flux increases as a function of time.

For arc-jet models, the in-depth thermal response on the centerline is often estimated by using a one-dimensional thermal response code, such as FIAT, and using the stagnation-point heat flux at the initial time [18,19]. That is, the effect of shape change on heat flux is not taken into account in the one-dimensional calculation. In Fig. 14, the predicted centerline temperatures at depths of 1.143, 1.524, 2.286, and 3.048 cm as predicted by TITAN-DPLR (with shape change) are compared with those computed by FIAT (without shape change). The in-depth temperature predictions using a simple one-dimensional approximation are significantly lower than the multidimensional loosely coupled simulation. This result is obtained because the constant heat flux boundary condition (808 W/cm^2) used in one-dimensional computation is lower than the true value (see Fig. 12),

and furthermore, the effect of radial conduction from side-wall heating is ignored in the one-dimensional calculation.

D. Case IV

The ablation and thermal response for an iso-q arc-jet model is studied in this case. The iso-q shape has a nose radius equal to the cylindrical diameter (10.16 cm) and a shoulder radius of 0.635 cm. The initial stagnation-point heat flux is 210 W/cm^2, and the stagnation-point pressure is 7 kPa. The DPLR CFD computation has a grid size of 221 × 149, and the TITAN simulation has a grid size of 223 × 160.

The predicted surface contours at 0, 70, and 140 s are shown in Fig. 15a, and the relative shape change after 140 s of exposure to the arc stream is plotted in Fig. 15b. A comparison of surface heating distributions between $t = 0$ and 140 s is presented in Fig. 16. Except for a moderate spike located on the shoulder region, the initial surface heat flux distribution is similar to the final distribution, and the stagnation heat flux remains almost unchanged throughout the entire heat pulse. The spike on the shoulder region goes away in the first 10 s of exposure time. The recession rate is fairly uniform over the

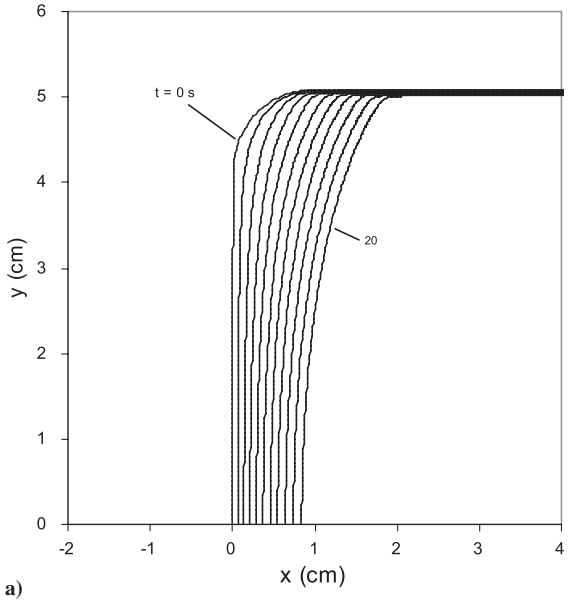

a)

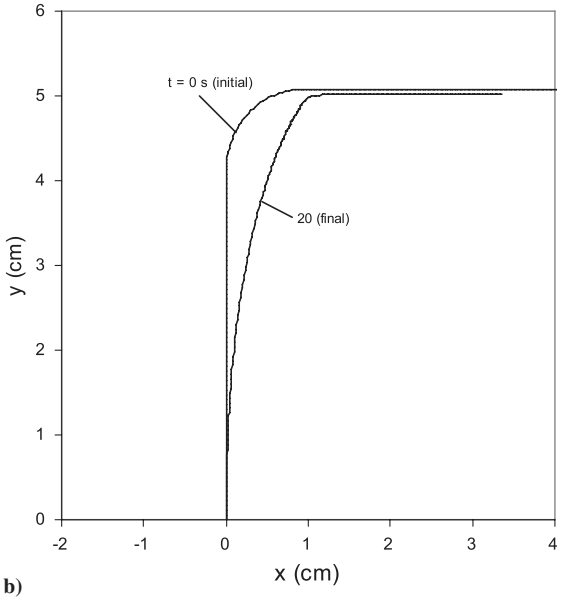

b)

Fig. 11 Plots of a) surface contours at various times for case III and b) relative shape change in 20 s of exposure for case III.

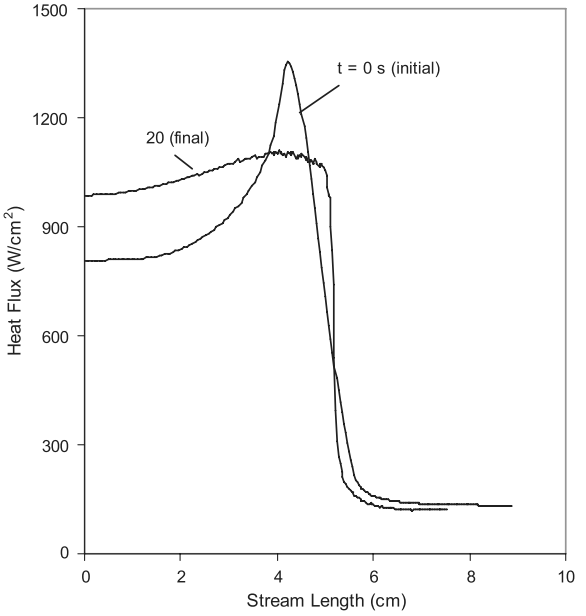

Fig. 12 Comparison of surface heat flux distributions at 0 and 20 s for case III.

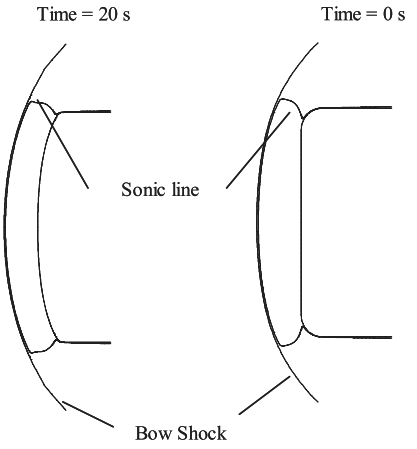

Fig. 13 Bow shock and sonic line for case III.

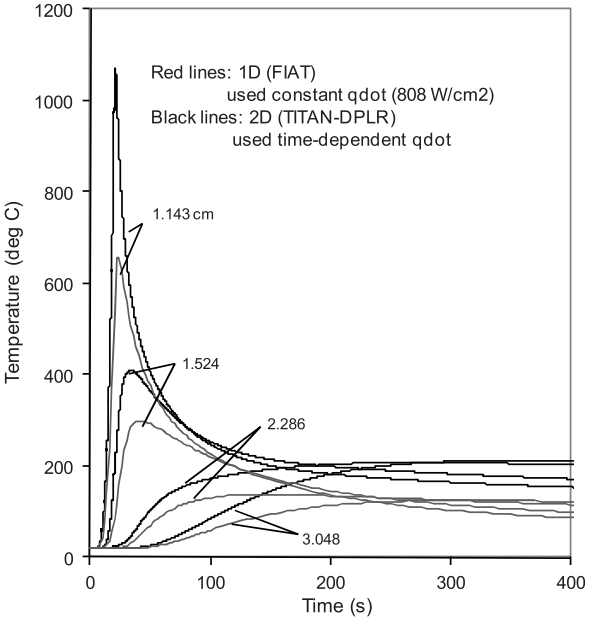

Fig. 14 Comparison of 1-D and 2-D in-depth temperature predictions for case III.

front surface. The body diameter recedes by a small amount as the result of side-wall heating, and the shoulder area has a minor shape correction. Overall, very little relative shape change is observed on most of the forward surface. In Fig. 17, the subsonic zone in front of the test model is presented. There is no significant change to shock shape and sonic line location at the end of heat pulse.

In [5], the modified surface heat flux distribution (shown in Fig. 18) was used as one of TITAN's time-dependent boundary conditions to predict the in-depth thermal response for this iso-q shape. This monotonically decreasing heating distribution was generated from a modified iso-q shape. This modified iso-q shape was semi-empirically built such that surface curvature increases (or radius of curvature decreases) away from stagnation point. As a result of the change in curvature, this modified shape produces relatively constant and monotonically decreasing surface heat flux. For those computations in [5], it was assumed that surface heat flux was not affected by the shape change throughout the entire heat pulse, and thus there was no need for loose coupling. In Fig. 19, a comparison of

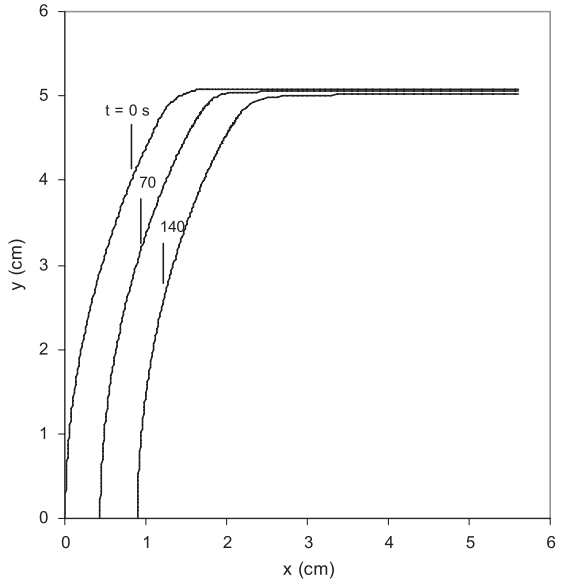

a)

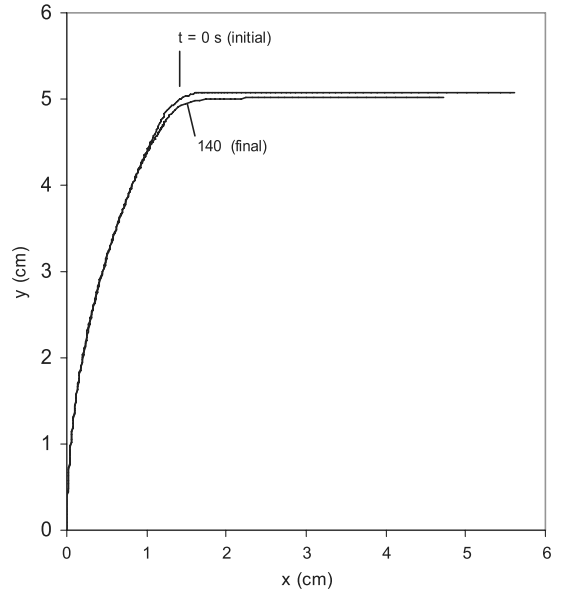

b)

Fig. 15 Plots of a) surface contours at various times for case IV and b) relative shape change in 140 s of exposure for case IV.

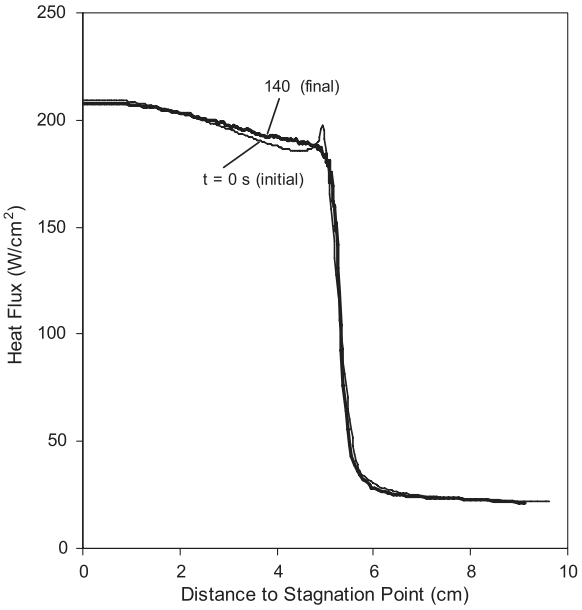

Fig. 16 Comparison of surface heat fluxes at 0 and 140 s for case IV.

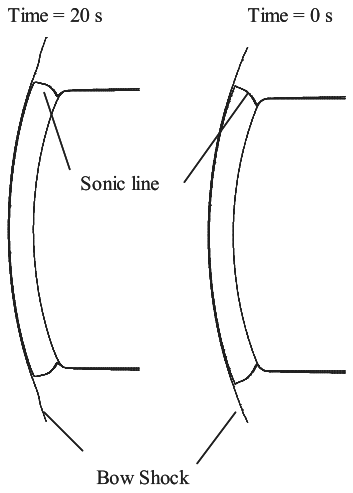

Fig. 17 Bow shock and sonic line for case IV.

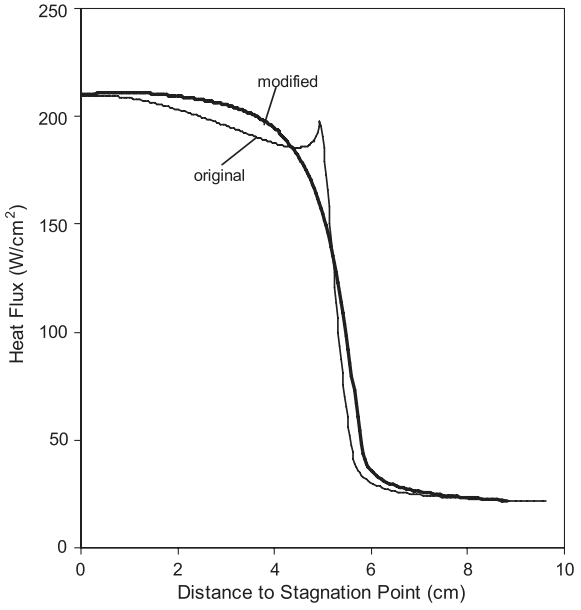

Fig. 18 Modified and unmodified heat flux distributions for case IV.

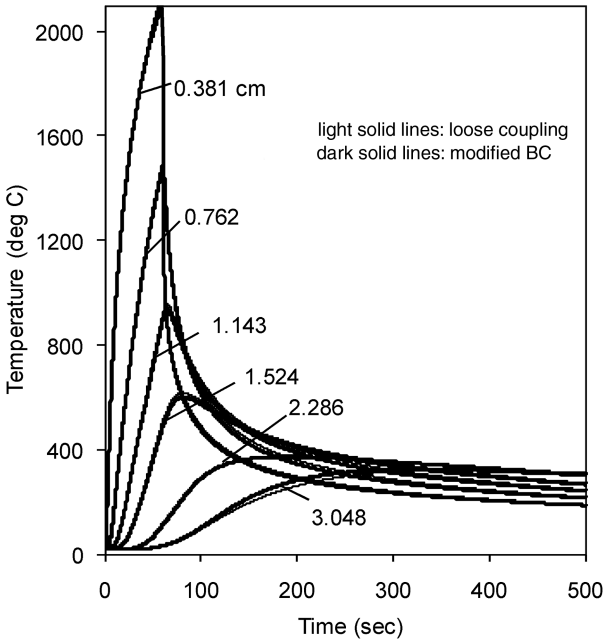

Fig. 19 Predicted in-depth temperature histories for case IV.

predicted centerline in-depth temperatures from the loosely coupled TITAN-DPLR computation (solid lines) and the previous TITAN computation with modified heat flux boundary condition (dark solid lines) is presented. The length of the heat pulse is 60 s. The predicted in-depth temperatures with the modified heat flux boundary condition are just slightly higher than those predicted using loose coupling. This is consistent with the observation that relative shape change of the iso-q model is small under this test condition. Thus, for some arc-jet cases, instead of performing a loosely coupled TITAN-DPLR computation, the relatively inexpensive alternative of running TITAN with the modified heat flux boundary condition may be used to predict the in-depth material thermal response with reasonable accuracy.

IV. Conclusions

Time-accurate solutions for pyrolysis, ablation, and shape change of thermal protection system materials were successfully obtained by loose coupling of the TITAN material response code with the DPLR computational fluid dynamics code. For a sample problem of hypersonic flow past a sphere cone, the agreement was excellent between shape change and heat flux predictions of the new TITAN-DPLR system and the old TITAN-GIANTS system. Depending on the number of processors used in the calculations, the computation time required by TITAN-DPLR is at least one order of magnitude less than that of the TITAN-GIANTS. This computation time savings is significant and may enable three-dimensional loosely coupled ablation simulations in the future.

Interaction between a hypersonic airstream and a two-dimensional 5° half-angle cylinder wedge at various angles of attack were performed to demonstrate the capabilities and to check the self-consistency of TITAN-DPLR system. The shape becomes more asymmetric as the AOA is increased. The predicted final stagnation heat fluxes are equivalent to a 13% reduction relative to the initial value.

We calculated the axisymmetric response of flat-faced and iso-q-shaped arc-jet models. For the flat-faced model, the heat flux distribution has a maximum near the shoulder. Therefore, the recession rate is greater near the shoulder than near the axis, and the relative shape change because of differential recession is significant. The flowfield changes as a function of time, and the heat flux magnitude and distribution are consequently altered. A simple one-dimensional simulation of conduction along the axis underpredicts in-depth temperature histories in comparison to a two-dimensional simulation that accounts for the change in heat transfer distribution due to shape change, the effects of side-wall heating and the anisotropic thermal conductivity of the material. For the iso-q shape, the initial heat flux distribution is relatively uniform, and the effects of differential recession are reduced. We compared a loosely coupled TITAN-DPLR computation with an uncoupled TITAN calculation, using a modified heat flux distribution. The results indicate that the uncoupled TITAN calculation can be used to replace the more expensive loose coupling between TITAN and DPLR for such cases in which the relative shape change is small.

Acknowledgment

The work was supported by the Orion TPS Advanced Development Project.

References

[1] Tran, H., Johnson, C., Rasky, D., Hui, F., Chen, Y.-K., and Hsu, M., "Phenolic Impregnated Carbon Ablators (PICA) for Discovery Class Missions," AIAA Paper 96-1911, June 1996.

[2] Willcockson, W. H., "Stardust Sample Return Capsule Design Experience," *Journal of Spacecraft and Rockets*, Vol. 36, No. 3, 1999, pp. 470–474. doi:10.2514/2.3468

[3] Greathouse, J. S., Kirk, B. S., Lillard, R. P., Truong, T. H., Robinson, P., and Cerimele, C. J., "Crew Exploration Vehicle (CEV) Crew Module Shape Selection Analysis and CEV Aerosciences Project Overview," AIAA Paper 2007-0603, Jan. 2007.

[4] Chen, Y.-K., and Milos, F. S., "Multi-Dimensional Effects on Heatshield Thermal Response for the Orion Crew Module," AIAA Paper 2007-4397, June 2007.

[5] Milos, F. S., and Chen, Y.-K., "Two-Dimensional Ablation, Thermal Response, and Sizing Program for Pyrolyzing Ablators," *Journal of Spacecraft and Rockets*, Vol. 46, No. 6, 2009, pp. 1089–1099. doi:10.2514/1.36575

[6] Chen, Y.-K., and Milos, F. S., "Ablation and Thermal Analysis Program for Spacecraft Heatshield Analysis," *Journal of Spacecraft and Rockets*, Vol. 36, No. 3, 1999, pp. 475–483. doi:10.2514/2.3469

[7] "User's Manual: Aerotherm Charring Material Thermal Response and Ablation Program," Aerotherm Div., Acurex Corp., Mountain View, CA, Aug. 1987.

[8] Chen, Y.-K., and Milos, F. S., "Two-Dimensional Implicit Thermal Response and Ablation Program for Charring," *Journal of Spacecraft and Rockets*, Vol. 38, No. 4, 2001, pp. 473–481. doi:10.2514/2.3724

[9] Rafinejad, D., Dahm, T. J., Brink, D. F., Abbett, M. J., and Wolf, C. J., "Passive Nosetip Technology (PANT II) Program Volume II. Computer User's Manual: ABRES Shape Change Code (ASCC)," U.S. Air Force Space and Missile Systems Organization Rept. TR-77-11, Mountain View, CA, Oct. 1976.

[10] Candler, G. V., and MacCormack, R. W., "Computation of Weakly Ionized Hypersonic Flows in Thermochemical Nonequilibrium," *Journal of Thermophysics and Heat Transfer*, Vol. 5, No. 3, 1991, pp. 266–273. doi:10.2514/3.260

[11] Dahm, T. J., Cooper, L., Rafinejad, D., Youngblood, S. B., and Kelly, J. T., "Passive Nosetip Technology (PANT II) Program Volume I. Inviscid Flow and Heat Transfer Modeling for Reentry Vehicle Nosetips," U.S. Air Force Space and Missile Systems Organization Rept. TR-77-11, Mountain View, CA, Oct. 1976.

[12] Wright, M. J., Candler, G. V., and Bose, D., "Data-Parallel Line Relaxation Method for the Navier–Stokes Equations," *AIAA Journal*, Vol. 36, No. 9, 1998, pp. 1603–1609. doi:10.2514/2.586

[13] Chen, Y.-K., and Milos, F. S., "Three-Dimensional Ablation and Thermal Response Simulation System," AIAA Paper 2005-5064, June 2005.

[14] Gökcen, T., Chen, Y.-K., Skokova, K. A., and Milos, F. S., "Computational Analysis of Arc-Jet Stagnation Tests Including Ablation and Shape Change," AIAA Paper 2009-3596, June 2009.

[15] Squire, T. H., Milos, F. S., and Hartlieb, G. C., "Aerospace Material Property Database (TPS*X*)," *Journal of Spacecraft and Rockets*, Vol. 46, No. 3, 2009, pp. 733–736. doi:10.2514/1.43777

[16] Kendall, R. M., "An Analysis of the Coupled Chemically Reacting Boundary Layer and Charring Ablator, Part V, A General Approach to

the Thermochemical Solution of Mixed Equilibrium-Nonequilibrium Homogeneous or Heterogeneous Systems," NASA CR-1064, 1968.

[17] Milos, F. S., and Chen, Y.-K., "Comprehensive Model for Multi-Component Ablation Thermochemistry," AIAA Paper 97-0141, Jan. 1997.

[18] Covington, M. A., Heinenmann, J. M., Goldstein, H. E., Chen, Y.-K., Terrazas-Salinas, I., Balboni, J. A., Olejniczak, J., and Martinez, E. R., "Erratum, Performance of a Low Density Ablative Heat Shield Material," *Journal of Spacecraft and Rockets*, Vol. 45, No. 4, 2008, pp. 854–864.
doi:10.2514/1.38249

[19] Covington, M. A., Heinenmann, J. M., Goldstein, H. E., Chen, Y.-K., Terrazas-Salinas, I., Balboni, J. A., Olejniczak, J., and Martinez, E. R., "Erratum, Erratum on Performance of a Low Density Ablative Heat Shield Material," *Journal of Spacecraft and Rockets*, Vol. 45, No. 6, 2008, pp. 1330–1330.
doi:10.2514/1.40598

K. Wurster
Associate Editor